Title

Revealing the Electrochemical Charging Mechanism of Nanosized Li2S by in Situ and Operando X-ray Absorption Spectroscopy

Journal

Nano Letters, 17(8)

ISSN

1530-6984

Authors

Zhang, Liang

Sun, Dan

Feng, Jun

et al.

Publication Date

2017-08-09

DOI

10.1021/acs.nanolett.7b02381

Peer reviewed

NANO LETTERS

Letter

pubs.acs.org/NanoLett

Revealing the Electrochemical Charging Mechanism of Nanosized Li_2S by in Situ and Operando X-ray Absorption Spectroscopy

Liang Zhang,[†,⊥] Dan Sun,[‡,⊥] Jun Feng,[†] Elton J. Cairns,*[,‡,§] and Jinghua Guo*[,†,∥]

[†]Advanced Light Source and [‡]Energy Technologies Area, Lawrence Berkeley National Laboratory, Berkeley, California 94720, United States

[§]Department of Chemical and Biomolecular Engineering, University of California, Berkeley, California 94720, United States

[∥]Department of Chemistry and Biochemistry, University of California, Santa Cruz, California 95064, United States

Supporting Information

ABSTRACT: Lithium sulfide (Li_2S) is a promising cathode material for lithium−sulfur (Li/S) cells due to its high theoretical specific capacity (1166 mAh g^{-1}) and ability to pair with nonmetallic lithium anodes to avoid potential safety issues. However, when used as the cathode, a high charging voltage (~4 V versus Li^+/Li) is always necessary to activate Li_2S in the first charge process, and the voltage profile becomes similar to that of a common sulfur electrode in the following charge processes. In this report, we have prepared an electrode of nanosphere Li_2S particles and investigated its charging mechanism of the initial two charge processes by in situ and operando X-ray absorption spectroscopy. The results indicate that Li_2S is directly converted to elemental sulfur through a two-phase transformation in the first charge process, while it is oxidized first to polysulfides and then to sulfur in the second charge process. The origin of the different charging mechanisms and corresponding charge-voltage profiles of the first and second charge processes is found to be related to the remaining polysulfides at the end of the first discharge process: they can not only facilitate the charge-transfer process at the Li_2S/electrolyte interface but also chemically react with Li_2S and act as the polysulfide facilitator for the electrochemical oxidation of Li_2S in the following charge processes. Our present study provides a new fundamental understanding of the charging mechanism of the Li_2S electrode, which should be of help for the further development of high-performance Li/S cells.

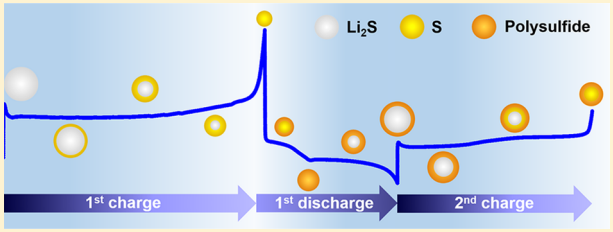

KEYWORDS: *Lithium batteries, lithium sulfide, energy storage, in situ and operando, X-ray absorption spectroscopy*

Lithium−sulfur (Li/S) cells have attracted remarkable attention in recent years due to their potentially higher capacity and specific energy compared to existing lithium-ion batteries (LIBs).[1−9] Assuming a complete conversion reaction ($16Li + S_8 \rightarrow 8Li_2S$), Li/S cells can deliver a theoretical specific energy of 2600 Wh kg^{-1}, which is five times higher than that of LIBs. Moreover, as a byproduct of the petroleum refining process, sulfur is naturally abundant, environmentally benign, and inexpensive. Therefore, Li/S cells are considered as one of the most-promising candidates for next-generation electrical energy storage systems for electric vehicles and large-area grids.[1−7]

Despite the advantages of high specific energy and low cost, there are still challenges for the practical utilization of Li/S cells.[1,4,5,10−12] The first one is the poor electrical conductivity of the reaction products (S_8 in the charged state and Li_2S in the discharged state). The second one is the high solubility of intermediate polysulfides (PSs) into organic electrolytes during both charge and discharge processes, which causes the "shuttle effect" and uncontrollable deposition of sulfur species on the lithium metal electrode. The typical strategy to address the challenges mentioned above is to encapsulate sulfur cathodes with conducting materials such as carbons or conducting polymers to improve the conductivity of cathode and trap the intermediate PSs.[1,5,13,14] Another challenge for Li/S cells is to use lithium metal as the anode, which typically forms dendrites in conventional organic solvent-based electrolytes and causes shorting and safety concerns.[15,16] In addition, the sulfur electrode suffers a large volume change during cycling (~80%), resulting in the mechanical degradation of the electrode.[4,5]

Given this, fully lithiated lithium sulfide (Li_2S, theoretical capacity: 1166 mAh g^{-1}) has attracted attention because much-safer anodes (e.g., silicon, aluminum, and tin) can be paired with Li_2S, which can avoid the dendrite problem and circumvent safety concerns associated with metallic lithium.[1,4,5,17−25] Moreover, Li_2S has a much higher melting point than that of sulfur (1372 versus 115 °C), allowing for the use of high-temperature heat treatment and material modification methods to protect Li_2S cathode and prevent PSs from dissolving in electrolytes. In addition, the mechanical

Received: June 5, 2017
Revised: July 19, 2017
Published: July 21, 2017

DOI: 10.1021/acs.nanolett.7b02381
Nano Lett. 2017, 17, 5084−5091

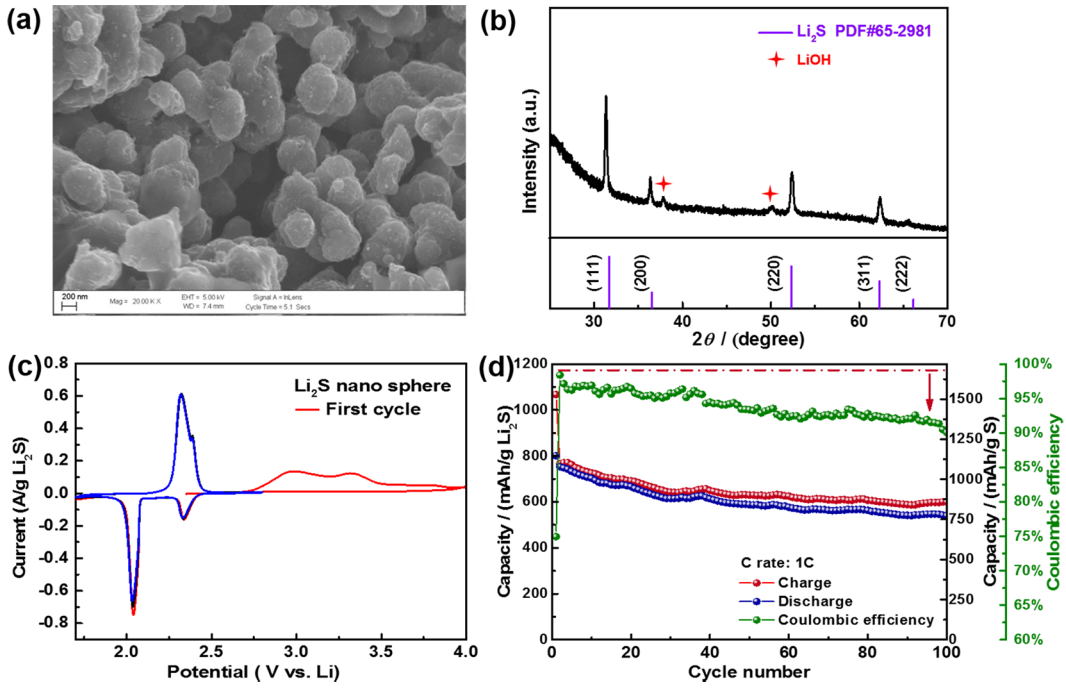

Figure 1. (a,b) SEM image and XRD pattern of the as-prepared nanosphere Li_2S particles. (c) Cyclic voltammograms of the Li_2S electrode at a scan rate of 0.025 mV/s. (d) Cycling performance and Coulombic efficiency of the Li_2S electrode between 1.7 and 2.8 V at a 1C rate.

damage of the cathode during charge and discharge cycles can be alleviated because Li_2S already occupies the maximum volume, and the empty space generated during the charge process can accommodate the volume expansion of sulfur during the discharge process.

Because Li_2S is in its fully lithiated state, it needs to be charged first to delithiate the Li_2S and convert it to sulfur. Specifically, a high charging voltage is always necessary to activate Li_2S in the very first charge process.[1,4,5,17−21,26−28] For example, Cui et al. demonstrated that commercial Li_2S (a ∼10 μm particle) could be activated by charging to 4 V versus Li^+/Li in the initial charge, and each subsequent charge could be performed at a lower voltage (3.5 V).[29] In addition, a large potential barrier at ∼3.5 V was observed in the initial charge process, which was ascribed to the phase-nucleation process of PSs.[29] The height of the potential barrier was also dependent on kinetic factors such as charge transfer between Li_2S and electrolyte and lithium-ion diffusivity in Li_2S. For example, through high-energy ball milling of commercial Li_2S with conductive carbon black, the potential barrier was reduced to ∼2.55 V due to the excellent contact between Li_2S and carbon black.[19] However, a charging voltage of 4 V was still required to fully convert Li_2S into sulfur although a much lower charging voltage (2.8 V) is required in the subsequent charge processes.[19] This raises the following question: what is the origin of the high charging voltage for activating the Li_2S electrode in the first charge process? To answer this question, a fundamental understanding of the charging mechanism of the Li_2S electrode is needed.

Considering the high sensitivity of Li_2S to moisture, in situ characterization methodologies are required to elucidate the evolution of Li_2S during the charge processes. Recently, in situ and operando X-ray diffraction (XRD) has been employed to characterize the phase evolution of Li_2S in the first charge process.[29,30] However, XRD is only capable of detecting crystalline solids but not amorphous species, which limits its application. X-ray absorption spectroscopy (XAS) is element-specific and capable of detecting species that are amorphous or crystalline. In addition, different sulfur species (such as elemental sulfur, Li_2S, and different PSs) can be clearly distinguished in S K-edge XAS spectra.[31−37] In this work, we have investigated the redox reactions of an electrode comosed of nanosphere Li_2S in real time by in situ and operando S K-edge XAS. By combining morphology characterization, electrochemistry investigation, and in situ and operando XAS techniques, we are able to reveal the distinct charging mechanism of Li_2S and determine the origin of the high charging voltage in the first charge process.

Figure 1a shows the scanning electron microscopy (SEM) image of the synthesized nanosphere Li_2S particles with a uniform size of ∼500 nm. The short diffusion length associated with the much smaller dimension of the nanosphere Li_2S compared with the commercial Li_2S can effectively reduce the diffusion distance of ions and electrons during charging in the solid state.[17] The X-ray diffraction (XRD) pattern of the prepared sample is displayed in Figure 1b. The XRD peaks observed in the XRD pattern correspond to the cubic structure of Li_2S (Fm3m, PDF no. 65-2981), which indicates that Li_2S was successfully formed and no side reactions occurred. The formation of LiOH was induced by the reaction of Li_2S with moisture during XRD measurement.

Cyclic voltammetry (CV) of the nanosphere Li_2S electrode was performed for 3 cycles at a slow scan rate of 0.025 mV/s with the potential swept from open-circuit voltage (OCV) to 4.0 V followed by sweeping between 1.7 and 2.8 V, and the corresponding results are shown in Figure 1c. The first anodic scan demonstrates two broad oxidation peaks, which are related to the energy barrier for the conversion of pristine Li_2S to sulfur.[19,26] In the subsequent cathodic scan, two reduction peaks centered at 2.3 and 2.1 V are observed, corresponding to the stepwise reduction of elemental sulfur to polysulfide intermediates and further to Li_2S.[19,26] One oxidation peak at

DOI: 10.1021/acs.nanolett.7b02381
Nano Lett. 2017, 17, 5084−5091

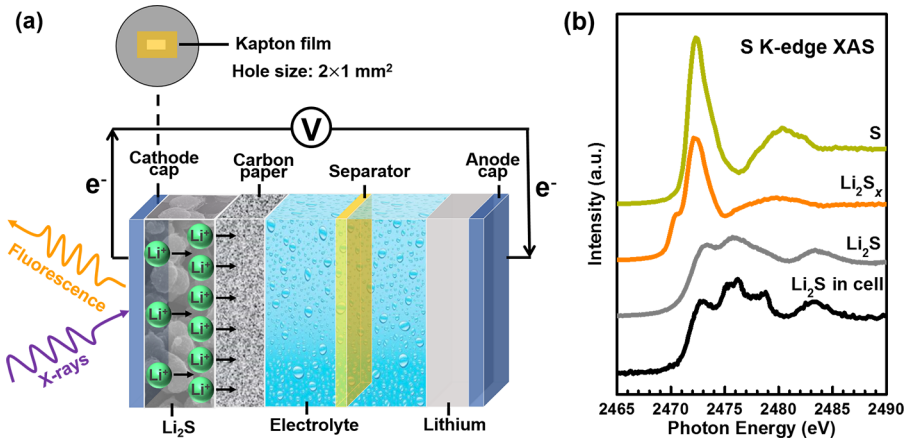

Figure 2. (a) Schematic depiction of the in situ coin cell for simultaneous cycling and X-ray spectroscopic measurement. (b) Reference XAS spectra of sulfur, PSs, and Li_2S, and XAS spectrum of the Li_2S electrode in the cell. The pre-edge feature at 2470.5 eV is identified as the fingerprint of PSs and is due to the terminal sulfur. The new features at 2476.2 and 2478.8 eV for the Li_2S electrode originate from the surface reaction of Li_2S with the electrolyte.

2.32 V with a shoulder is developed in the second anodic scan, which is associated with the conversion of Li_2S to sulfur.[1,26] The different oxidation peak positions between the first and second anodic scans of the Li_2S cathode strongly indicate the different reaction mechanisms. The cycling performance and Coulombic efficiency of the Li_2S electrode are shown in Figure 1d. A charging capacity of 1083.7 mAh g^{-1} was delivered after the first charge process, which is close to the theoretical value of 1166 mAh g^{-1}. However, a capacity of only 800 mAh g^{-1} was obtained after the first discharge process due to the loss of active electrode material. After 100 cycles, the discharge capacity decayed to 538 mAh g^{-1} and the Coulombic efficiency gradually dropped to 90%, mainly due to the "shuttle effect" of polysulfides.

To better understand the reaction mechanism of the nanosphere Li_2S electrode during the charge and discharge processes, an in situ and operando XAS experiment was conducted. The cells used to perform the in situ and operando XAS study were adapted from CR2325 coin cells (Figure 2a): a 2 × 1 mm^2 hole was drilled at the cathode side of the cell housing using a high-precision laser system, and the hole was sealed using a 20 μm thick Kapton film to allow X-ray beam penetration. Owing to the inherent elemental sensitivity of XAS, the signal from the Kapton film that is exposed to X-rays does not contribute any feature to the S K-edge XAS spectra collected through the X-ray window. As demonstrated in the results below, the design implemented here allows direct X-ray measurements under normal electrochemical operation.

Figure 2b shows the reference XAS spectra of α-S_8, PSs, and Li_2S. The XAS spectrum of α-S_8 shows a strong peak at 2472.2 eV, which is assigned to the high-intensity "white line" (1s to 3p transition) of element sulfur.[31,33] For PSs, in addition to the main feature at 2472.2 eV, a pre-edge feature at 2470.5 eV appears, which is attributed to the terminal S atoms, i.e., those at the end of polysulfide dianion chains.[31] In the following analysis of the in situ and operando S K-edge XAS spectra, we will identify the formation of PSs by the appearance of this pre-edge feature. The XAS spectrum of Li_2S exhibits two main features at ~2473.2 and ~2475.7 eV, respectively, which is consistent with previous reports.[32,33] In contrast, the XAS spectrum of the Li_2S electrode in the coin cell with $LiClO_4$ as the lithium salt at OCV shows two additional features at 2476.2 and 2478.8 eV besides the main Li_2S peaks, which are attributed to Li_2S–SO_3 and Li_2SO_3, respectively.[38,39] We propose that the presence of these two species originates from the surface oxidation of Li_2S particles by contact with $LiClO_4$. To check the validity of our assumption, we also measured the XAS spectra of the Li_2S electrode assembled with different lithium salts (i.e., $LiNO_3$, $LiFP_6$, and LiTFSI) (Figure S2). Interestingly, these two species are observed in all the XAS spectra (except the spectrum of LiTFSI, due to the overlap between the positions of sulfone groups in LiTFSI and Li_2SO_3).[39] Moreover, the intensities of these two features are different when using different lithium salts, with the highest intensities for $LiClO_4$. This is consistent with the fact that $LiClO_4$ is the strongest oxidant among the four lithium salts.[40] Overall, these experimental results clearly indicate that the lithium salts can slightly oxidize Li_2S to Li_2S–SO_3 and Li_2SO_3, although the main species of the electrode is still Li_2S.

Figure 3a shows the in situ and operando S K-edge XAS spectra for the Li_2S electrode during the first charge process at a C/15 rate with a cutoff voltage of 4.0 V. Similar to previous reports, the voltage profile (Figure 3d) shows a barrier (peak) at 2.9 V followed by a long flat plateau at ~2.7 V, following which the voltage rises to 4.0 V.[19,29] The total capacity extracted in the first charge process is 1080 mAh g^{-1}, indicating that almost all of the Li_2S has been converted to sulfur in the activation process. The XAS spectral shape changes significantly during the charging process. Specifically, the intensity of the peak at 2473.2 eV is continuously increasing during charging due to the conversion reaction from Li_2S to sulfur. However, at the very end of charge (uppermost spectrum in Figure 3b), the peak position of sulfur is different from that of α-S_8 shown in Figure 2b, which may indicate the formation of a new crystalline phase of sulfur (e.g., β-S_8) or an amorphous phase of sulfur.[30,41] Also, no feature is observed at 2470.5 eV, indicative of the absence of PS intermediates throughout the first charging process. Note that a similar phenomenon was also observed in the first charge of commercial Li_2S by the same method.[33] However, in that report, the XAS spectral features were not quantified and the reason for the requirement of a high charging voltage in the first charge process was not discussed.[33] It is worth mentioning that the evolution of the features at 2478.8 and 2482.2 eV is due to the oxidation of Li_2S

DOI: 10.1021/acs.nanolett.7b02381
Nano Lett. 2017, 17, 5084–5091

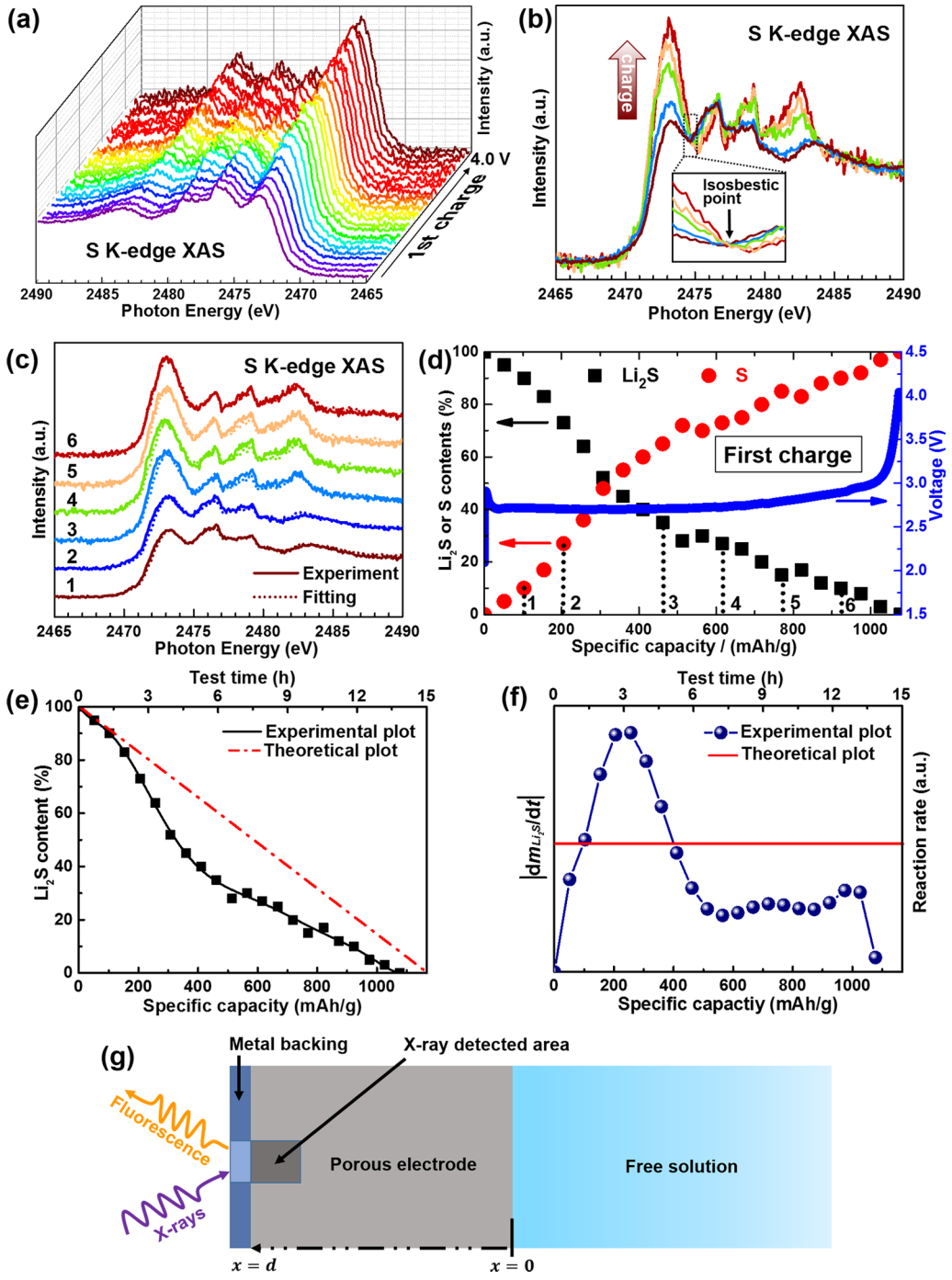

Figure 3. Operando S K-edge XAS spectra of the nanosphere Li_2S cathode for the first charge process. (a) S K-edge XAS spectra collected simultaneously with electrochemical cycling at a C/15 rate. (b) Selected XAS spectra during the charge process. The inset shows the presence of an isosbestic point. (c) Comparison of the experimental (solid lines) and two-phase fitting (dotted lines) of the XAS spectra. (d) Contents of sulfur and Li_2S calculated from two-phase fitting of the XAS spectra as a function of specific capacity. The values of the contents are obtained directly from the fitting parameters of the two-phase fitting spectra. For example, the values marked by numbers 1 to 6 correspond to the fitting parameters of the spectra shown in (c). The charge voltage profile during the operando XAS measurement is also plotted. (e) The fitting (black line) and theoretical (red line) content of Li_2S as a function of specific capacity. (f) The reaction rate of Li_2S ($|\frac{d_{mLi_2S}}{d_t}|$) as a function of specific capacity. The red line shows the theoretical reaction rate of the whole Li_2S electrode. (g) Schematic illustration of one-dimensional porous electrode model.

to Li_2SO_3 and Li_2SO_4 by electrochemical reactions, which is reversible during the charge and discharge processes (see figures below).

More information is obtained from the stack plot of XAS spectra at different charge stages, as shown in Figure 3b. The plot shows the presence of an isosbestic point for the XAS spectra (inset of Figure 3b).[42,43] Such an isosbestic point indicates the dominating two-phase transformation in the first charge process, which is consistent with the charge voltage profile. The quantitative analysis of the evolution of Li_2S and sulfur in the electrode at different charge stages is obtained by constructing the simulated spectra for the intermediate states

DOI: 10.1021/acs.nanolett.7b02381
Nano Lett. 2017, 17, 5084−5091

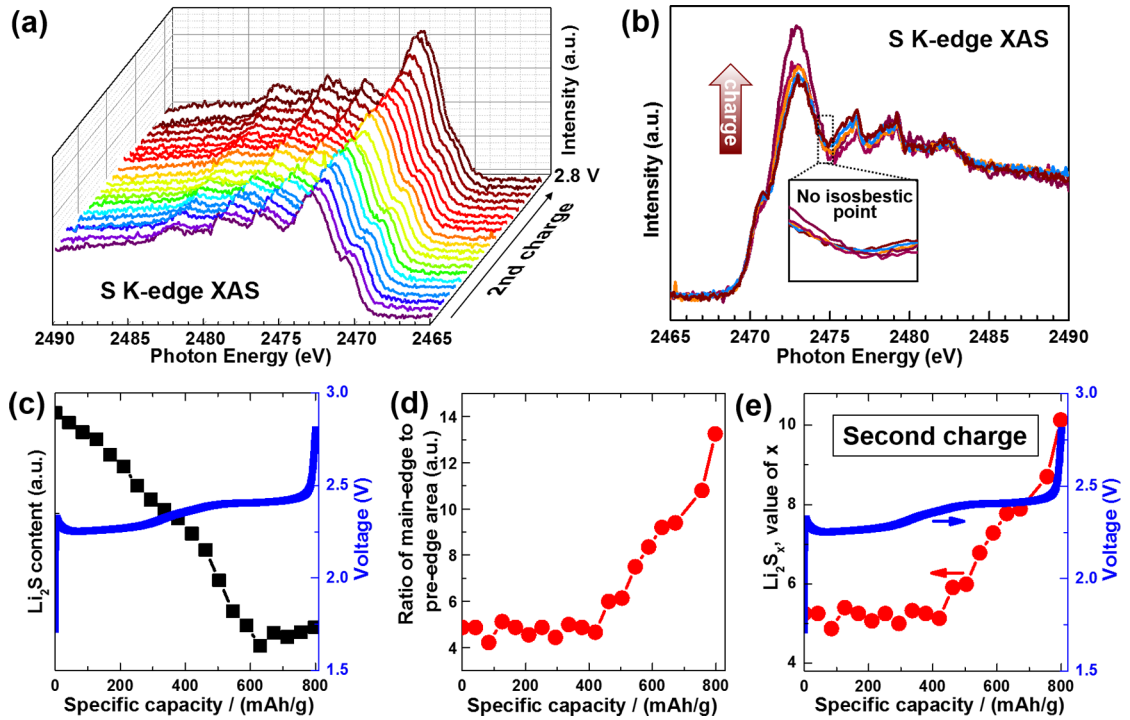

Figure 4. Operando S K-edge XAS spectra of the nanosphere Li_2S electrode for the second charge process. (a) S K-edge XAS spectra collected simultaneously with electrochemical cycling with a C/10 rate. (b) Selected XAS spectra during the charge process. The inset shows no isosbestic point. (c) The content of Li_2S as a function of specific capacity represented by the normalized intensity related to Li_2S feature at 2475.7 eV. (d) The ratio of main-edge peak area to pre-edge peak area based on fitting of the experimental spectra shown in (a). (e) The average chain length of PSs as a function of specific capacity. The charge voltage profile during the operando XAS measurement is also shown.

using linear combinations of the spectra of the initial and final states. The fitting results (dotted lines in Figure 3c) show an excellent agreement with the experimental data (solid lines in Figure 3c), confirming the two-phase scenario of the conversion of Li_2S to sulfur in the first charge process.

The contents of Li_2S and sulfur obtained directly from the fitting parameters of the two-phase fitting spectra as a function of charge capacity are displayed in Figure 3d, along with the charge curve during the operando XAS measurement. The content of Li_2S decreases monotonously as a function of charge capacity, which is contrary to that of sulfur. Based on the results present above, we propose the following charge mechanism. In contrast to the assumption that long-chain PSs are the main oxidation products for commercial Li_2S,[19,29] we propose that sulfur is the final charged species of our nanosphere Li_2S formed through a two-phase transformation. Note that the different final reaction products may be related to the different sizes of commercial Li_2S and our nanosphere Li_2S. Because Li_2S is an ionic crystal, the strong bonding strength between Li^+ and S^{2-} makes it difficult to extract Li^+ from Li_2S into the electrolyte.[17,29] Consequently, a high overpotential is necessary to overcome the barrier of Li^+ extraction. Note that the charge rate and charge-transfer process at the surface of Li_2S can also influence the value of the overpotential, as demonstrated by Yang et al.[29] In the initial charge process, the lithium ions are mainly extracted from the outer part of the nanosphere Li_2S, and the diffusion distance is relatively short. As the charging process proceeds, the electrochemically generated sulfur accumulates on top of unreacted Li_2S and forms a core–shell-like structure. Such structure can not only increase the diffusion distance of lithium ions but also lead to a larger charge-transfer resistance, as reflected by the gradual increase of overpotential in the voltage profile (Figure 3d). At the end of charge, all Li_2S disappears and only the sulfur phase exists, and therefore, the whole first charge is a solid → solid reaction. Because there is no PS formed and, thus, no "shuttle effect", high specific capacity can always be achieved for the Li_2S electrode in the first charge process.[1,4,5]

Here, it is worth mentioning that ideally the content change of Li_2S should keep a linear relationship with the specific capacity and the reaction rate of Li_2S ($|\frac{d_{mLi_2S}}{d_t}|$) should be constant during the whole charge process (indicated by red lines in Figure 3e and f), which is clearly not the case for the experiment results. This discrepancy is related to the nonuniform reaction distribution in the Li_2S electrode.[44−46] Due to the limited X-ray detection depth in the Li_2S electrode, the content change of Li_2S calculated based on XAS results only reflects the local change in the X-ray detected area, while the specific capacity represents the conversion from Li_2S to sulfur of the whole electrode. To better understand the actual−ideal discrepancy, it is useful to consider the Li_2S electrode as an one-dimensional porous electrode with uniform geometry and polarization parameters, as shown in Figure 3g.[46,47] At the electrode−solution phase boundary ($x = 0$), all of the current is carried by the electrolyte, while at the electrode−metal backing phase boundary ($x = d$), all of the current is carried by a conductive matrix.[46] Because the total current density is specified in our case (C/15), to maintain a constant current density on the whole electrode, local current density and reaction distribution in each depth of electrode ($0 \le x \le d$) are different and determined by polarization, both electronic and ionic conductivity of the two phases, and also the state of charge.[46,47] As a consequence, the content of Li_2S in the

DOI: 10.1021/acs.nanolett.7b02381
Nano Lett. 2017, 17, 5084−5091

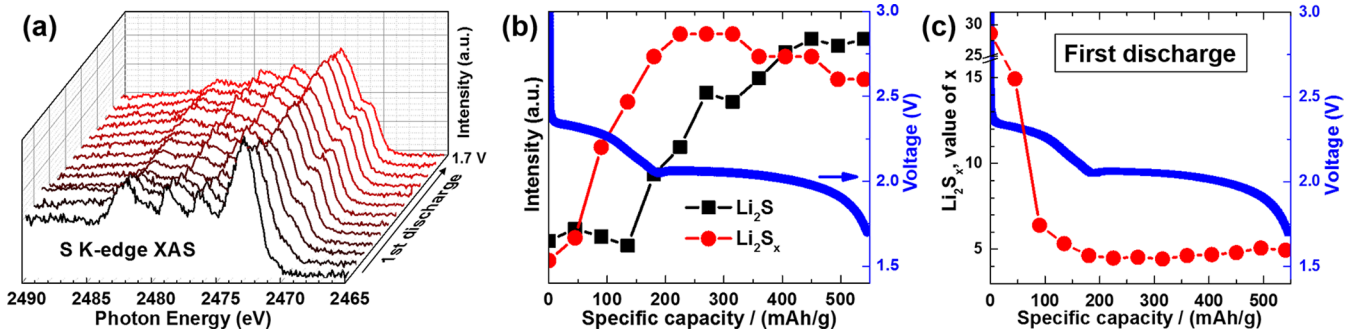

Figure 5. Operando S K-edge XAS spectra of the nanosphere Li_2S cathode for the first discharge process. (a) S K-edge XAS spectra collected simultaneously with electrochemical cycling at a C/10 rate. (b) The contents of Li_2S and PSs as a function of specific capacity represented by the normalized intensity related to Li_2S feature at 2475.7 eV and the normalized intensity of the fingerprint feature of PSs at 2470.5 eV, respectively. (c) The average chain length of PSs as a function of specific capacity. The discharge voltage profile during the operando XAS measurement is also shown.

detected area does not change linearly with the amount of charge passed by the whole Li_2S electrode. In addition, the reaction rate of Li_2S in the detected area varies with time (Figure 3f), which should result from the change in the local state of charge during the electrochemical process.

Having clarified the reaction mechanism of the first charge process, we now examine the details of the second charge process. The specific capacity of the second charge at a C/10 rate is 803 mAh g^{-1} (69% of the theoretical capacity), with an overpotential that is much lower than that of first charge. Similar to the first charge, the in situ and operando S K-edge XAS spectra (Figure 4a) of the second charge also demonstrate a gradual increase of the feature at ~2473 eV due to the transformation from Li_2S to sulfur. Interestingly, a new pre-edge feature at 2470.5 eV known as the fingerprint of PSs is observed even in the initial XAS spectrum, while no such feature is observed in the whole first charge process. In addition, no isosbestic point is present in the XAS spectra (Figure 4b), suggesting that the second charge process is not a two-phase reaction and the reaction mechanism is different for the first and second charge process due to the absence and presence of PSs.

To elucidate the role of PSs, the evolution of different sulfur species upon the second charge process is discussed next. As shown in Figure 4c, Li_2S is consumed monotonically during most of the charging process, which is consistent with previous reports.[30,32] In contrast, due to the overlap of the main XAS features of sulfur and various PSs, it is technically difficult to distinguish between them.[33] Instead, we use the main-edge to pre-edge peak area ratio as the proxy for the average chain length of PSs at different charge stages (Figure 4d), given that the cathode material is composed of PSs with a distribution of lengths.[34] By using the linear relationship between the spectral features and average chain length of PSs ($y = 0.5824x + 2.4133$, where x is average chain length and y is the ratio of main-edge to pre-edge area),[34] we can directly convert the area ratio into the average chain length of PSs, as demonstrated in Figure 4e. The value of x shows a weak function of capacity when the capacity is lower than 420 mAh g^{-1} and then increases from 5.1 to 10.2 continuously afterward. The initial x value of 5.2 again corroborates the presence of PSs at the very beginning of the second charge (the x value should be 1 if there is no PSs). Because of the presence of PSs in the electrolyte, extracting Li^+ from Li_2S to the electrolyte is much easier considering the fact that the bonding environment of Li^+ in Li_2S is more similar to that in PSs than in pure electrolyte, resulting in the decrease of overpotential in the two-plateau charge voltage profile (Figure 4e).[29] In addition, these PSs can also play a role of polysulfide nuclei for the following electrochemical reaction.[29] Notably, the voltage profile of the second charge becomes similar to the charge profile of common sulfur electrode, consistent with a similar reaction mechanism for them.[1,5]

For the sulfur electrode, Cuisinier et al. have found that the oxidation of Li_2S formed in the first discharge proceeded in a straightforward manner through the soluble intermediates of S_4^{2-} and S_6^{2-} to solid sulfur by electrochemical reaction.[32] Therefore, the average chain length of PSs should increase as a function of capacity, inconsistent with our results. Actually, the PSs can not only decrease the overpotential but also chemically react with Li_2S to form short-chain PSs (for example, $2Li_2S + 3Li_2S_6 \rightarrow 5Li_2S_4$).[33,34] Due to the presence of both electrochemical and chemical reactions, the average chain length is almost constant at the early stage of the second charge process. With the consumption of Li_2S, the electrochemical reaction is dominant, leading to the increase of the average chain length to 10.2. In principle, the x value at the end of charge should be infinity because all Li_2S is oxidized to sulfur. The x value of 10.2 here may result from the incomplete conversion from Li_2S or PSs to sulfur or the imperfect fitting of the pre-edge and main-edge features in XAS spectra.[30,32,34] From the discussion above we can conclude that, due to the presence of PSs at the very beginning of the second charge, the overpotential in the voltage profile gets smaller and the whole charge process is a solid → liquid → solid reaction. The presence of PSs in the electrolyte induces the "shuttle effect", leading to capacity fading and lower Coulombic efficiency.

However, the origin of these PSs in the initial second charge process is still unclear. We have therefore similarly investigated the first discharge process using in situ and operando XAS to learn about the origin of the PSs, as shown in Figure 5a. The main feature at ~2473 eV is also strongly affected by discharge due to the cleavage of S−S bonds. In addition, the fingerprint feature of PSs at 2470.5 eV appears at the intermediate stages of discharge. Figure 5b shows the intensity trend of Li_2S and PSs as a function of discharge capacity as well as the voltage profile at a C/10 rate. The discharge voltage profile displays the typical two-plateau behavior of the sulfur electrode, where a discharge capacity of 548 mAh g^{-1} is obtained. It is believed that these two plateaus correspond to the conversion of sulfur to long-chain PSs ($S_8 \rightarrow Li_2S_8 \rightarrow Li_2S_6 \rightarrow Li_2S_4$) and long-chain PSs to

DOI: 10.1021/acs.nanolett.7b02381
Nano Lett. 2017, 17, 5084−5091

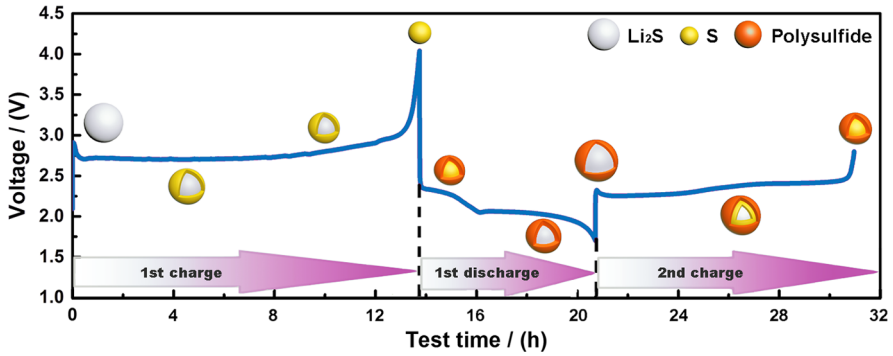

Figure 6. Proposed reaction scheme of the Li_2S electrode during the initial charge and discharge processes. Note that the polysulfides can be dissolved in the electrolyte, resulting in the "shuttle effect".

short-chain polysulfides ($Li_2S_4 \rightarrow Li_2S_2 \rightarrow Li_2S$), respectively.[1,4,5] As seen in Figure 5b, the relative fraction of terminal sulfur atoms in PSs dramatically increases when transitioning from the higher to lower voltage plateau and then gradually decreases in the following process, in good agreement with the conversion process of sulfur during discharge.[1,4,5] In addition, the Li_2S species is formed only starting from the lower-voltage plateau, which is consistent with other in situ and operando reports.[30,36]

To gain the deeper insight into the sulfur reduction mechanism, we have calculated the average chain length x of PSs at different discharge stages using the method described above (Figures 5c and S3). The value of x drops steeply from 28.9 to 4.7 in the higher discharge plateau and then becomes nearly constant in the lower discharge plateau. The initial x value of 28.9 in the discharge process again indicates that sulfur is the main oxidation product in the first charge process. The value of x at the end of the higher discharge plateau is 4.7, which is a little larger than the theoretical value 4.[1,5] This observation may indicate the presence of some unreacted sulfur at this stage.[32] Moreover, the chemical reaction between sulfur and short-chain PSs (e.g., $S_8 + 2Li_2S_4 \rightarrow 2Li_2S_8$) can also result in an increase of the average chain length of PSs.[34] At the end of the lower discharge plateau, the average chain length is 4.9, much larger than the theoretical value of 1 (supposing that Li_2S is the final reduction product) but very close to that of PSs at the beginning of the second charge (i.e., 5.1). This result indicates that, on the one hand, not all PSs are reduced to Li_2S in the final stage of the first discharge, and on the other hand, the initial PSs in the second charge originate from the residual PSs from the first discharge.

Based on the discussion above, the reaction mechanism of the Li_2S cathode in Li/S cells during the initial charge and discharge processes can be summarized as shown in Figure 6. In the first charge process, Li_2S is directly oxidized to sulfur through a two-phase solid−solid transformation. Because the first charge process is a solid → solid reaction, a high overpotential is necessary to extract Li^+ from Li_2S into the electrolyte due to the strong bonding between Li^+ and S^{2-}. In the subsequent discharge process, sulfur is reduced first to PSs and then to Li_2S through both electrochemical and chemical reactions. However, only a part of the PSs is reduced to Li_2S in the final stage of first discharge process. For the second charge process, due to the presence of PSs at the beginning of charge, the charge-transfer process at the Li_2S surface is fast, leading to a lower overpotential in the voltage profile. In addition, the PSs also chemically react with Li_2S and facilitate the electrochemical reaction of Li_2S, which results in a different reaction mechanism (solid → liquid → solid reaction) from that of the first charge process. However, the accumulation of unreacted PSs along with cycling can result in both lower sulfur utilization and the "shuttle effect" as reported by many researchers: only 68.2% of the initial discharge capacity is retained after 100 cycles accompanied by a decreasing Coulombic efficiency (Figure 1d).

In conclusion, we have synthesized nanosphere Li_2S particles and used them as the positive electrode material of Li/S cells, which show the high specific capacity and good cyclability. Furthermore, we investigated the redox mechanism of this electrode in real time throughout the initial two charge cycles by in situ and operando XAS. In the first charge cycle, Li_2S is directly converted to elemental sulfur via a two-phase reaction without the formation of polysulfides. Therefore, the first charge process is a solid to solid reaction and a high charging voltage is essential to fully extract Li^+ from Li_2S into the electrolyte, considering the fact that Li_2S is an ionic crystal. In contrast, polysulfides are observed at the very beginning of the second charge, which originate from the residual polysulfides formed in the first discharge process. These polysulfides mainly have three effects: (i) reducing the charge-transfer resistance at the Li_2S/electrolyte interface and thus leading to a lower overpotential in the voltage profile; (ii) acting as polysulfide facilitator for the electrochemical reaction of Li_2S; and (iii) chemically reacting with Li_2S to form short-chain polysulfides. As a consequence, in the second charge process Li_2S is first oxidized to polysulfides and then to sulfur through both electrochemical and chemical reactions that correspond to a solid → liquid → solid reaction. Our current study provides a new fundamental understanding of the charge mechanism of the Li_2S electrode and highlights the double-sided role of polysulfides in the electrochemical processes, which can facilitate the further development of high-performance Li/S cells with improved sulfur utilization and cycle life.

■ ASSOCIATED CONTENT

Supporting Information

The Supporting Information is available free of charge on the ACS Publications website at DOI: 10.1021/acs.nanolett.7b02381.

Additional details on experimental methods. Figures showing XAS spectra (PDF)

■ AUTHOR INFORMATION

Corresponding Authors

*E-mail: jguo@lbl.gov.

DOI: 10.1021/acs.nanolett.7b02381
Nano Lett. 2017, 17, 5084−5091

*E-mail: ejcairns@lbl.gov.

ORCID

Liang Zhang: 0000-0002-3446-3172
Elton J. Cairns: 0000-0002-1179-7591
Jinghua Guo: 0000-0002-8576-2172

Author Contributions

⊥L.Z. and D.S. contributed equally to this work.

Notes

The authors declare no competing financial interest.

■ ACKNOWLEDGMENTS

The work at Advanced Light Source and Molecular Foundry of the Lawrence Berkeley National Laboratory was supported by the Director, Office of Science, Office of Basic Energy Sciences, of the U.S. Department of Energy under contract no. DE-AC02-05CH11231. Work in the Energy Technologies Area of Lawrence Berkeley National Laboratory was supported by CERDEC U.S. ARMY under project no. 104302.

■ REFERENCES

(1) Seh, Z. W.; Sun, Y.; Zhang, Q.; Cui, Y. *Chem. Soc. Rev.* **2016**, *45*, 5605.
(2) Tao, X.; Wang, J.; Liu, C.; Wang, H.; Yao, H.; Zheng, G.; Seh, Z. W.; Cai, Q.; Li, W.; Zhou, G.; Zu, C.; Cui, Y. *Nat. Commun.* **2016**, *7*, 11203.
(3) Li, W.; Zhang, Q.; Zheng, G.; Seh, Z. W.; Yao, H.; Cui, Y. *Nano Lett.* **2013**, *13*, 5534.
(4) Yang, Y.; Zheng, G.; Cui, Y. *Chem. Soc. Rev.* **2013**, *42*, 3018.
(5) Manthiram, A.; Fu, Y.; Chung, S. H.; Zu, C.; Su, Y. S. *Chem. Rev.* **2014**, *114*, 11751.
(6) Rosenman, A.; Markevich, E.; Salitra, G.; Aurbach, D.; Garsuch, A.; Chesneau, F. F. *Adv. Energy Mater.* **2015**, *5*, 1500212.
(7) Bruce, P. G.; Freunberger, S. A.; Hardwick, L. J.; Tarascon, J. M. *Nat. Mater.* **2012**, *11*, 19.
(8) Pang, Q.; Liang, X.; Kwok, C. Y.; Nazar, L. F. *Nat. Energy* **2016**, *1*, 16132.
(9) Liang, X.; Kwok, C. Y.; Lodi-Marzano, F.; Pang, Q.; Cuisinier, M.; Huang, H.; Hart, C. J.; Houtarde, D.; Kaup, K.; Sommer, H.; Brezesinski, T.; Janek, J.; Nazar, L. F. *Adv. Energy Mater.* **2016**, *6*, 1501636.
(10) Ji, L.; Rao, M.; Zheng, H.; Zhang, L.; Li, Y.; Duan, W.; Guo, J.; Cairns, E. J.; Zhang, Y. *J. Am. Chem. Soc.* **2011**, *133*, 18522.
(11) Fang, R.; Zhao, S.; Sun, Z.; Wang, D. W.; Cheng, H. M.; Li, F. *Adv. Mater.* **2017**, 1606823.
(12) Yin, Y. X.; Xin, S.; Guo, Y. G.; Wan, L. J. *Angew. Chem., Int. Ed.* **2013**, *52*, 13186.
(13) Peng, H. J.; Zhang, G.; Chen, X.; Zhang, Z. W.; Xu, W. T.; Huang, J. Q.; Zhang, Q. *Angew. Chem., Int. Ed.* **2016**, *55*, 12990.
(14) Wang, Z.; Dong, Y.; Li, H.; Zhao, Z.; Wu, H. B.; Hao, C.; Liu, S.; Qiu, J.; Lou, X. W. *Nat. Commun.* **2014**, *5*, 5002.
(15) Cheng, X. B.; Zhang, R.; Zhao, C. Z.; Wei, F.; Zhang, J. G.; Zhang, Q. *Adv. Sci.* **2016**, *3*, 1500213.
(16) Li, W.; Yao, H.; Yan, K.; Zheng, G.; Liang, Z.; Chiang, Y. M.; Cui, Y. *Nat. Commun.* **2015**, *6*, 7436.
(17) Nan, C.; Lin, Z.; Liao, H.; Song, M. K.; Li, Y.; Cairns, E. J. *J. Am. Chem. Soc.* **2014**, *136*, 4659.
(18) Son, Y.; Lee, J.-S.; Son, Y.; Jang, J.-H.; Cho, J. *Adv. Energy Mater.* **2015**, *5*, 1500110.
(19) Cai, K.; Song, M. K.; Cairns, E. J.; Zhang, Y. *Nano Lett.* **2012**, *12*, 6474.
(20) Hwa, Y.; Zhao, J.; Cairns, E. J. *Nano Lett.* **2015**, *15*, 3479.
(21) Wang, C.; Wang, X.; Yang, Y.; Kushima, A.; Chen, J.; Huang, Y.; Li, J. *Nano Lett.* **2015**, *15*, 1796.
(22) Zhou, G.; Tian, H.; Jin, Y.; Tao, X.; Liu, B.; Zhang, R.; Seh, Z. W.; Zhuo, D.; Liu, Y.; Sun, J.; Zhao, J.; Zu, C.; Wu, D. S.; Zhang, Q.; Cui, Y. *Proc. Natl. Acad. Sci. U. S. A.* **2017**, *114*, 840.
(23) Qiu, Y.; Rong, G.; Yang, J.; Li, G.; Ma, S.; Wang, X.; Pan, Z.; Hou, Y.; Liu, M.; Ye, F.; Li, W.; Seh, Z. W.; Tao, X.; Yao, H.; Liu, N.; Zhang, R.; Zhou, G.; Wang, J.; Fan, S.; Cui, Y.; Zhang, Y. *Adv. Energy Mater.* **2015**, *5*, 1501369.
(24) Seh, Z. W.; Wang, H.; Liu, N.; Zheng, G.; Li, W.; Yao, H.; Cui, Y. *Chem. Sci.* **2014**, *5*, 1396.
(25) Wang, L.; Wang, Y.; Xia, Y. *Energy Environ. Sci.* **2015**, *8*, 1551.
(26) Sun, D.; Hwa, Y.; Shen, Y.; Huang, Y.; Cairns, E. J. *Nano Energy* **2016**, *26*, 524.
(27) Zhou, G. M.; Sun, J.; Jin, Y.; Chen, W.; Zu, C. X.; Zhang, R. F.; Qiu, Y. C.; Zhao, J.; Zhuo, D.; Liu, Y. Y.; Tao, X. Y.; Liu, W.; Yan, K.; Lee, H. R.; Cui, Y. *Adv. Mater.* **2017**, *29*, 1603366.
(28) Zhou, G. M.; Paek, E.; Hwang, G. S.; Manthiram, A. *Adv. Energy Mater.* **2016**, *6*, 1501355.
(29) Yang, Y.; Zheng, G.; Misra, S.; Nelson, J.; Toney, M. F.; Cui, Y. *J. Am. Chem. Soc.* **2012**, *134*, 15387.
(30) Waluś, S.; Barchasz, C.; Bouchet, R.; Leprêtre, J.-C.; Colin, J.-F.; Martin, J.-F.; Elkaïm, E.; Baehtz, C.; Alloin, F. *Adv. Energy Mater.* **2015**, *5*, 1500165.
(31) Wujcik, K. H.; Pascal, T. A.; Pemmaraju, C. D.; Devaux, D.; Stolte, W. C.; Balsara, N. P.; Prendergast, D. *Adv. Energy Mater.* **2015**, *5*, 1500285.
(32) Cuisinier, M.; Cabelguen, P.-E.; Evers, S.; He, G.; Kolbeck, M.; Garsuch, A.; Bolin, T.; Balasubramanian, M.; Nazar, L. F. *J. Phys. Chem. Lett.* **2013**, *4*, 3227.
(33) Gorlin, Y.; Patel, M. U. M.; Freiberg, A.; He, Q.; Piana, M.; Tromp, M.; Gasteiger, H. A. *J. Electrochem. Soc.* **2016**, *163*, A930.
(34) Wujcik, K. H.; Wang, D. R.; Pascal, T. A.; Prendergast, D.; Balsara, N. P. *J. Electrochem. Soc.* **2017**, *164*, A18.
(35) Gorlin, Y.; Siebel, A.; Piana, M.; Huthwelker, T.; Jha, H.; Monsch, G.; Kraus, F.; Gasteiger, H. A.; Tromp, M. *J. Electrochem. Soc.* **2015**, *162*, A1146.
(36) Lowe, M. A.; Gao, J.; Abruña, H. D. *RSC Adv.* **2014**, *4*, 18347.
(37) Pascal, T. A.; Wujcik, K. H.; Velasco-Velez, J.; Wu, C.; Teran, A. A.; Kapilashrami, M.; Cabana, J.; Guo, J.; Salmeron, M.; Balsara, N.; Prendergast, D. *J. Phys. Chem. Lett.* **2014**, *5*, 1547.
(38) Lin, Z.; Nan, C.; Ye, Y.; Guo, J.; Zhu, J.; Cairns, E. J. *Nano Energy* **2014**, *9*, 408.
(39) Li, X.; Lushington, A.; Sun, Q.; Xiao, W.; Liu, J.; Wang, B.; Ye, Y.; Nie, K.; Hu, Y.; Xiao, Q.; Li, R.; Guo, J.; Sham, T. K.; Sun, X. *Nano Lett.* **2016**, *16*, 3545.
(40) Jow, T. R.; Xu, K.; Borodin, O.; Makoto, U. *Electrolytes for lithium and lithium-ion batteries*; Springer: New York, 2014; Vol. *58*.
(41) Jha, H.; Buchberger, I.; Cui, X.; Meini, S.; Gasteiger, H. A. *J. Electrochem. Soc.* **2015**, *162*, A1829.
(42) Liu, X.; Liu, J.; Qiao, R.; Yu, Y.; Li, H.; Suo, L.; Hu, Y. S.; Chuang, Y. D.; Shu, G.; Chou, F.; et al. *J. Am. Chem. Soc.* **2012**, *134*, 13708.
(43) Wang, X.-J.; Jaye, C.; Nam, K.-W.; Zhang, B.; Chen, H.-Y.; Bai, J.; Li, H.; Huang, X.; Fischer, D. A.; Yang, X.-Q. *J. Mater. Chem.* **2011**, *21*, 11406.
(44) Zhang, G.; Shaffer, C. E.; Wang, C.-Y.; Rahn, C. D. *J. Electrochem. Soc.* **2013**, *160*, A610.
(45) Liu, X.; Wang, D.; Liu, G.; Srinivasan, V.; Liu, Z.; Hussain, Z.; Yang, W. *Nat. Commun.* **2013**, *4*, 2568.
(46) Newman, J. S.; Tobias, C. W. *J. Electrochem. Soc.* **1962**, *109*, 1183.
(47) Newman, J.; Tiedemann, W. *AIChE J.* **1975**, *21*, 25.

DOI: 10.1021/acs.nanolett.7b02381
Nano Lett. 2017, 17, 5084−5091